First-principles calculations of the nonlinear optical susceptibilities and Raman scattering spectra of lithium niobate

2007 J. Phys.: Condens. Matter 19 456202

(http://iopscience.iop.org/0953-8984/19/45/456202)

IOP PUBLISHING JOURNAL OF PHYSICS: CONDENSED MATTER

J. Phys.: Condens. Matter **19** (2007) 456202 (13pp) doi:10.1088/0953-8984/19/45/456202

First-principles calculations of the nonlinear optical susceptibilities and Raman scattering spectra of lithium niobate

P Hermet, M Veithen and Ph Ghosez

Physique Théorique des Matériaux, Université de Liège, B-5, 4000 Sart-Tilman, Belgium

Received 18 July 2007, in final form 24 September 2007
Published 11 October 2007
Online at stacks.iop.org/JPhysCM/19/456202

Abstract

Nonlinear optical susceptibilities and nonresonant Raman scattering spectra of the ferroelectric phase of lithium niobate ($LiNbO_3$) are computed using a first-principles approach based on density functional theory and taking advantage of a recent implementation based on the nonlinear response formalism and the $2n+1$ theorem. Infrared reflectivity spectra of the ferroelectric phase of $LiNbO_3$ are also calculated. New assignments are proposed for the E-modes, clarifying a longstanding debate in the literature. In addition, it is shown that knowledge of the nonlinear optical susceptibility tensor of $LiNbO_3$ does not significantly alter the profile of its Raman spectra in a configuration where the longitudinal optic modes are involved.

1. Introduction

Lithium niobate ($LiNbO_3$) belongs to the class of ferroelectric oxides. It is nowadays widely used due to its promising applications in various nonlinear optical and electro-optic devices [1–4]. However, to improve the performances of such devices, a better understanding of the microscopic physical properties of $LiNbO_3$, like its optic phonon modes, is required.

$LiNbO_3$ is a uniaxial crystal belonging to the trigonal system. Above 1480 K it is paraelectric and belongs to the rhombohedral space group $R\bar{3}c$. At 1480 K it undergoes a structural phase transition, and below that temperature it crystallizes in a ferroelectric rhombohedral structure of space group $R3c$. These two rhombohedral phases have 10 atoms and two formula units per primitive unit cell [5].

Raman spectroscopy is one of the experimental techniques that has been widely used for studying the phonon dynamics and the phase transition of $LiNbO_3$. However, in spite of the numerous experimental investigations during the last decade on its ferroelectric phase, the assignment of phonon modes of E symmetry is not yet unambiguously established in the literature and some controversies remain between the authors due to the presence of both intrinsic and extrinsic defects in $LiNbO_3$ crystals [6, 7]. In addition, even the previous first-principles calculations do not manage to clarify these controversies because only the frequency

positions of the calculated Raman lines are considered to assign the experimental spectra, the intensities of the Raman lines not being reported in previous works [8, 9].

In this paper we calculate, for several configurations, the Raman spectra of the ferroelectric phase of $LiNbO_3$ including both the frequency position and the intensity of Raman lines. For this purpose, we use density functional theory (DFT), taking advantage of a recent implementation based on the nonlinear response formalism and the $2n+1$ theorem [10, 11]. The computation of the intensity of the Raman lines has been performed not only for the transverse optical (TO) modes, but also for the longitudinal optical (LO) modes. Infrared reflectivity spectra of the ferroelectric phase of $LiNbO_3$ are also calculated. These calculations allow unambiguous assignment of all the experimental Raman lines to specific phonon modes, and succeed in clarifying the longstanding debate in the literature relating to the assignment of the E-modes.

This paper is organized as follows. Sections 2 and 3, respectively, describe the theoretical formalism and the computational parameters used to compute the nonlinear optical susceptibility tensors and the nonresonant Raman spectra of $LiNbO_3$. In section 4, we present our computational results. We report the nonlinear optical susceptibility tensors of the ferroelectric phase of $LiNbO_3$, a quantity required to compute the intensity of the LO Raman lines. Then, we show that the Raman spectra of the $R3c$ phase of $LiNbO_3$, obtained from first principles, are sufficiently accurate to be compared to the experimental ones and are relevant for the assignment of the experimental lines. In particular, a new assignment of the Raman lines of E symmetry, based on the analysis of the Raman intensities and mode oscillator strengths, is proposed. Calculated infrared reflectivity spectra of $LiNbO_3$ are also reported. In addition, a discussion about the influence of the nonlinear optical susceptibility coefficients on the calculation of the Raman intensity of the LO lines is also given in this section. Finally, our results are summarized in section 5.

2. Theoretical section

2.1. Nonlinear optical susceptibility tensor

In an insulator the polarization, $\boldsymbol{P}$, can be expressed as a Taylor expansion of the macroscopic electric field, $\boldsymbol{\mathcal{E}}$, according to

$$P_i = P_i^s + \sum_j \chi_{ij}^{(1)} \mathcal{E}_j + \sum_{j,l} \chi_{ijl}^{(2)} \mathcal{E}_j \mathcal{E}_l + \cdots, \tag{1}$$

where indices i, j, l denote the Cartesian components, $\boldsymbol{P}^s$ is the zero-field (spontaneous) polarization vector, $\tilde{\chi}^{(1)}$ is the linear dielectric susceptibility (second-rank tensor) and $\tilde{\chi}^{(2)}$ is the second-order nonlinear optical susceptibility (third-rank tensor). In the literature on nonlinear optics, instead of using the $\tilde{\chi}^{(2)}$-tensor, one often prefers to use the $\tilde{d}$-tensor defined as: $\tilde{d} = \frac{1}{2}\tilde{\chi}^{(2)}$.

Experimentally, the optical linear and nonlinear susceptibilities correspond to measurements for electric fields at frequencies high enough to get rid of the ionic relaxation but low enough to avoid electronic excitations. In the case of the second-order susceptibilities, this constraint implies that both the frequency of $\boldsymbol{\mathcal{E}}$ and of its second harmonic are lower than the fundamental absorption gap.

At the theoretical level, the optical linear and nonlinear susceptibilities are assimilated into the electronic response of the system that should *a priori* depend on the frequencies of the optical electric fields [12]. In the present context of the $2n + 1$ theorem applied within the local density approximation to (static) DFT, we neglect the dispersion of $\tilde{\chi}^{(2)}$, computing the electronic response at zero frequency. As a consequence, the $\chi_{ijl}^{(2)}$ tensor elements satisfy

the Kleinman symmetry condition [13] and are therefore symmetric under a permutation of indices i, j and l. Following the works of Dal Corso and co-workers [14, 15], we can relate the nonlinear optical susceptibilities to a third-order derivative of a field-dependent energy functional $\mathcal{F} = E - \Omega_0 \boldsymbol{\mathcal{E}} \cdot \boldsymbol{P}$, where Ω_0 and E are, respectively, the unit cell volume and the total energy in zero field. Practical details concerning how $\tilde{\chi}^{(2)}$ can be computed by a linear response taking advantage of the $2n + 1$ theorem are reported in [10].

2.2. Nonresonant Raman scattering

The nonresonant Raman scattering efficiency in a given direction, with a frequency between ω_d and $\omega_d + \mathrm{d}\omega_d$, and within a solid angle $\mathrm{d}\Omega$, is given for a Stokes process by [16]:

$$\frac{\mathrm{d}^2 S}{\mathrm{d}\Omega\, \mathrm{d}\omega_d} = \frac{\omega_d^4}{16\pi^2 c^4}[B(\omega) + 1]\hbar \sum_{i,j,k,l} v_i v_k I_{ijkl}(\omega) w_j w_l, \tag{2}$$

where $\omega = \omega_0 - \omega_d$ and

$$I_{ijkl}(\omega) = \sum_{\mathrm{m}} a^{\star}_{ij}(m) a_{kl}(m) \frac{1}{2\omega_{\mathrm{m}}}[\delta(\omega - \omega_{\mathrm{m}}) - \delta(\omega + \omega_{\mathrm{m}})]. \tag{3}$$

In these equations, indices i, j, k, l denote the Cartesian components, the asterisk symbolizes the complex conjugation, c is the speed of light in the medium, $\hbar$ is the reduced Planck constant, ω_0 (resp. ω_d) is the frequency of incident (resp. scattered) light, $\boldsymbol{v}$ (resp. $\boldsymbol{w}$) is the polarization unit vector of the incident (resp. scattered) light, $B(\omega)$ is the Bose factor and ω_{m} is the frequency of the mth zone-center phonon mode. The Raman susceptibility tensor is defined as

$$a_{ij}(m) = \sqrt{\Omega_0} \sum_{\kappa,\gamma} \pi^{\kappa}_{ij,\gamma}\, u_{\mathrm{m}}(\kappa\gamma), \tag{4}$$

where the sum runs over all atoms κ and space directions γ, $u_{\mathrm{m}}(\kappa\gamma)$ is the $(\kappa\gamma)$-component of the mth phonon eigendisplacement vector and $\tilde{\pi}$ is a third-rank tensor describing the changes of the linear dielectric susceptibility induced by an individual atomic displacement defined as

$$\pi^{\kappa}_{ij,\gamma} = \left.\frac{\partial \chi^{(1)}_{ij}}{\partial \tau_{\kappa\gamma}}\right|_0, \tag{5}$$

where $\tau_{\kappa\gamma}$ corresponds to the displacement of the κth atom in the direction γ.

The dynamical matrix, yielding the phonon frequencies and eigendisplacements, was obtained within a variational approach to density functional perturbation theory [17].

For TO phonons ($\mathcal{E} = 0$), $\tilde{\pi}$ can be computed as a mixed third-order derivative of the energy functional, $\mathcal{F}$, with respect to an electric field, twice, and to an atomic displacement under the condition of zero electric field:

$$\pi^{\kappa}_{ij,\gamma}|_{\mathcal{E}=0} = -\frac{6}{\Omega_0} \mathcal{F}^{\tau_{\kappa\gamma}\mathcal{E}_i\mathcal{E}_j}. \tag{6}$$

Table 1 reports the independent elements of the $\tilde{\pi}$-tensor for the TO modes related to the asymmetric unit of the $R3c$ phase of $LiNbO_3$. Knowledge of these can be relevant for computing the electro-optic coefficients of $LiNbO_3$ or for further theoretical Raman studies of this material using for instance the bond polarizability model [18]. $\tilde{\pi}$-tensors for the other atoms can be obtained from those given in table 1 applying the symmetry operations expected by the $R3c$ space group.

For the case of LO phonons ($\mathcal{D} = 0$) with wavevector $\boldsymbol{q} \to \boldsymbol{0}$ in a polar crystal, equation (4) must additionally take into account the effect of the macroscopic electric field generated by the

Table 1. $\pi^{\kappa}_{ij,\gamma}$ tensor elements of the TO modes ($\times 10^{-3}$ Bohr^{-1}) related to the asymmetric unit of the $R3c$ phase of $LiNbO_3$.

	γ		
κ	x	y	z
Li	$\begin{pmatrix} -4.1 & -6.9 & 7.5 \\ -6.9 & 4.1 & -11.2 \\ 7.5 & -11.2 & 0.0 \end{pmatrix}$	$\begin{pmatrix} -6.9 & 4.1 & 11.2 \\ 4.1 & 6.9 & 7.5 \\ 11.2 & 7.5 & 0.0 \end{pmatrix}$	$\begin{pmatrix} 2.6 & 0.0 & 0.0 \\ 0.0 & 2.6 & 0.0 \\ 0.0 & 0.0 & 0.1 \end{pmatrix}$
Nb	$\begin{pmatrix} 22.9 & -19.8 & -86.3 \\ -19.8 & -22.9 & -36.0 \\ -86.3 & -36.0 & 0.0 \end{pmatrix}$	$\begin{pmatrix} -19.8 & -22.9 & 36.0 \\ -22.9 & 19.8 & -86.3 \\ 36.0 & -86.3 & 0.0 \end{pmatrix}$	$\begin{pmatrix} -86.1 & 0.0 & 0.0 \\ 0.0 & -86.1 & 0.0 \\ 0.0 & 0.0 & -191.6 \end{pmatrix}$
O	$\begin{pmatrix} -58.3 & -7.6 & 41.2 \\ -7.6 & -22.4 & 8.0 \\ 41.2 & 8.0 & -62.8 \end{pmatrix}$	$\begin{pmatrix} 9.8 & -5.4 & 4.3 \\ -5.4 & 26.1 & 11.3 \\ 4.3 & 11.3 & 18.2 \end{pmatrix}$	$\begin{pmatrix} 37.4 & 10.8 & -37.3 \\ 10.8 & 18.3 & 1.1 \\ -37.3 & 1.1 & 63.8 \end{pmatrix}$

lattice polar vibration. This field enters in the computation of the Raman susceptibilities at two levels. On one hand it gives rise to the non-analytical part of the dynamical matrix that modifies the frequencies and eigenvectors with respect to pure TO phonons. On the other hand, the electric field induces an additional change in the dielectric susceptibility tensor related to the nonlinear optical coefficients $\chi^{(2)}_{ijk}$. Thus, for LO phonons, equation (6) has to be modified as follows [19]:

$$\pi^{\kappa}_{ij,\gamma}|_{\mathcal{D}=0} = \pi^{\kappa}_{ij,\gamma}|_{\mathcal{E}=0} - \frac{8\pi}{\Omega_0} \frac{\sum_l Z^*_{\gamma l}(\kappa) q_l}{\sum_{l,l'} q_l \varepsilon^{\infty}_{ll'} q_{l'}} \sum_l \chi^{(2)}_{ijl} q_l, \tag{7}$$

where $\mathcal{D}$ is the electric displacement vector, $\tilde{Z}^*(\kappa)$ is the Born effective charge tensor of the κth atom and $\tilde{\varepsilon}^{\infty}$ is the optical dielectric tensor. For $\tilde{Z}^*$ and $\tilde{\varepsilon}^{\infty}$ tensors, we used values from a previous work [20]. Practical details concerning how the $\tilde{\pi}$-tensors can be computed by linear response are described in [10]. As we discuss further below, the accuracy in the calculation of frequencies and $\tilde{\pi}$-tensors will be respectively estimated from a direct comparison between the experimental frequency positions and the intensities of the $LiNbO_3$ Raman lines. For all the calculated Raman spectra shown in this paper, the Raman line shape is assumed to be Lorentzian and the linewidth is fixed at 4 cm^{-1}.

3. Computational details

Our first-principles studies of the ferroelectric phase of $LiNbO_3$ were performed in the framework of DFT, as implemented in the ABINIT package [21]. Structural relaxation was done until the maximum residual forces (stresses) were less than 10^{-5} Ha Bohr^{-1} (10^{-7} Ha Bohr^{-3}). The relaxed parameters, given in [20], are in close agreement with previous first-principles calculations and experimental data. The exchange–correlation energy functional was evaluated within the local density approximation (LDA) as parametrized by Perdew and Wang [22]. The all-electron potentials were replaced by norm-conserving pseudopotentials generated according to the Troullier–Martins scheme [23] thanks to a package developed at the Fritz-Haber Institute (Berlin) [24]. Niobium (4s, 4p, 4d, 5s), lithium (1s, 2s) as well as oxygen (2s, 2p) electrons were considered as valence states in the construction of the pseudopotentials. Convergence of the structure optimization and phonon calculation were reached for a 45 Ha plane-wave kinetic energy cut-off and a $6 \times 6 \times 6$ mesh of special k-points [25], whereas 35 Ha and a $8 \times 8 \times 8$ mesh were required to converge the $\tilde{d}$-tensor and $\tilde{\pi}$-tensor elements.

Table 2. Independent elements of the $\tilde{d}$-tensor (in pm V^{-1}) of $LiNbO_3$.

	d_{31}	d_{22}	d_{33}
Present	−8.01	−1.23	−30.21
Exp. [26]	−4.64	+2.46	−41.7
Exp. [19]	−6.75	+3.6	−37.5

4. Results and discussions

4.1. Nonlinear optical susceptibility tensor

In this subsection, we give the nonlinear optical susceptibility tensor, $\tilde{d}$, that will be used in the following to compute the Raman intensities of the LO lines. In the ferroelectric phase of $LiNbO_3$, the $\tilde{d}$-tensor has four independent elements given by (in Voigt notation)

$$d_{ij} = \begin{pmatrix} 0 & 0 & 0 & 0 & d_{15} & -d_{22} \\ -d_{22} & d_{22} & 0 & d_{15} & 0 & 0 \\ d_{31} & d_{31} & d_{33} & 0 & 0 & 0 \end{pmatrix}. \tag{8}$$

The Kleinman symmetry rule allows us to reduce this tensor to three independent elements, since in this case we have $d_{31} = d_{15}$. The elements of the $\tilde{d}$-tensor calculated in the ferroelectric phase of $LiNbO_3$ are given in table 2 and are compared to the experimental values[1]. We observe a reasonable agreement between the theoretical and experimental values. Nevertheless, although all calculated susceptibilities are found to be negative, a positive value has been experimentally reported for d_{22}. Nonlinear optical susceptibilities are particularly difficult to measure accurately and the values reported by different authors are often in substantial disagreement [27]. Thus, as the sign is unambiguously defined in our calculations, we suggest that the positive sign of d_{22} reported experimentally might result from a wrong interpretation of the experimental measurements.

4.2. Assignment of the Raman spectra

The zone-center optical phonon modes of the $R3c$ phase of $LiNbO_3$ can be classified, according to its irreducible representations, into $4A_1 \oplus 5A_2 \oplus 9E$. The A_1-modes polarized along z and the doubly degenerate E-modes polarized in the x–y plane are both Raman and infrared active while the A_2-modes are silent. If the orthogonal reference system (x, y, z) is chosen as such as z is aligned along the polar axis of $LiNbO_3$ ([111] pseudocubic direction) and x aligned along the crystallographic a-axis, the Raman susceptibility tensors of the A_1- and E-modes have a well-defined form given, respectively, by [28]:

$$A_1(z) = \begin{pmatrix} a & 0 & 0 \\ 0 & a & 0 \\ 0 & 0 & b \end{pmatrix}, \tag{9}$$

$$E(x) = \begin{pmatrix} c & 0 & d \\ 0 & -c & 0 \\ d & 0 & 0 \end{pmatrix}, \qquad E(y) = \begin{pmatrix} 0 & -c & 0 \\ -c & 0 & d \\ 0 & d & 0 \end{pmatrix}. \tag{10}$$

4.2.1. A-modes. The computed frequencies of the five A_2-modes are 218, 297, 412, 454 and 892 cm^{-1}. Those obtained for the A_1(TO) and A_1(LO) modes are given in table 3.

[1] Contrary to what is usually achieved within LDA, a very good agreement was also reported between the experimental and theoretical linear optical susceptibilities [20] that can be explained by the unusually small LDA error on the electronic band gap.

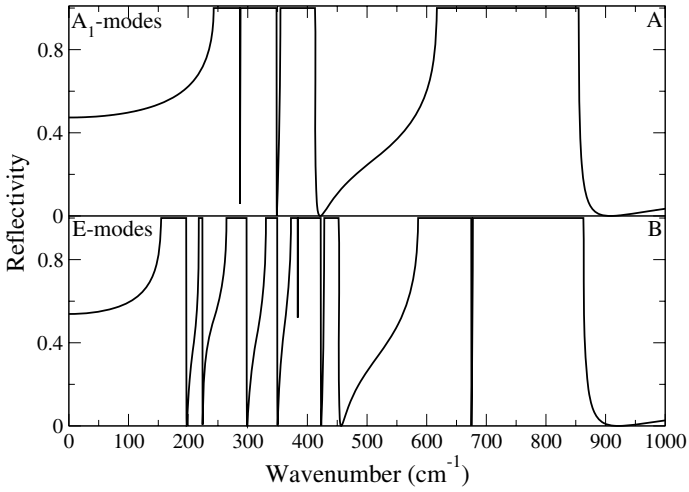

Figure 1. Calculated infrared reflectivity spectra of $LiNbO_3$ for the A_1-modes (A) and E-modes (B) in the 0–1000 cm^{-1} range.

Table 3. Overlap matrix between the eigenvectors of the A_1(LO) and A_1(TO) modes of $LiNbO_3$. Values in parentheses are the frequencies (in cm^{-1}) of the different A_1-modes whereas the values in square brackets are the mode effective charges of the A_1(TO)-modes.

		TO1 [6.946] (243)	TO2 [0.526] (288)	TO3 [1.131] (355)	TO4 [6.577] (617)
LO1	(287)	0.156	**0.995**	0.015	−0.013
LO2	(348)	0.365	−0.073	**0.932**	−0.092
LO3	(413)	**0.811**	−0.127	−0.372	−0.450
LO4	(855)	0.446	−0.057	−0.091	**0.897**

Calculated frequencies for both A_1- and A_2-modes are close to those reported experimentally and theoretically in the literature [7, 29–33]. Table 3 also reports the mode effective charges given by [17]

$$Z^*_{m,\alpha} = \left(\sum_{\kappa,\beta} Z^*_{\alpha\beta}(\kappa) u_{\mathrm{m}}(\kappa\beta)\right) \Bigg/ \left(\sqrt{\sum_{\kappa,\beta} u^2_{\mathrm{m}}(\kappa\beta)}\right), \tag{11}$$

and the overlap matrix between the eigenvectors of the A_1(LO) and A_1(TO) modes defined as

$$\langle \mathbf{u}^{\mathrm{LO}}_{\mathrm{m}} | \tilde{M} | \mathbf{u}^{\mathrm{TO}}_{n} \rangle = \sum_{\beta,\kappa} u^{\mathrm{LO}}_{\mathrm{m}}(\kappa\beta) M_\kappa u^{\mathrm{TO}}_{n}(\kappa\beta), \tag{12}$$

where M_κ is the mass of the κth atom, and $\mathbf{u}^{\mathrm{LO}}$ and $\mathbf{u}^{\mathrm{TO}}$ are, respectively, the eigendisplacement vectors of the A_1(LO) and A_1(TO) modes. Indeed, due to the long-range Coulomb interaction, the eigenvectors of the TO modes do not necessarily correspond to those of the LO modes.

Panel A of figure 1 displays the calculated infrared reflectivity spectrum (without damping) at normal incidence of the A_1-modes. This spectrum was obtained as described in [17]. A good agreement between theory and experiment [29] is observed both for frequency and minima positions. Although figure 1 suggests that the three lowest modes exhibit a similar LO/TO splitting, the inspection of table 3 shows that the TO1 and TO4 modes exhibit a giant LO/TO

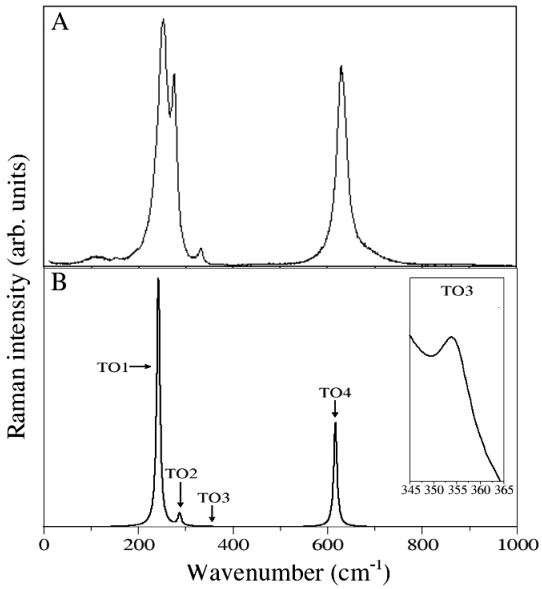

Figure 2. Experimental [33] (A) and calculated (B) Raman spectra of $LiNbO_3$ for a $x(zz)y$ scattering configuration in the 0–1000 cm^{-1} range. Inset: zoom of the calculated spectrum in the 345–365 cm^{-1} range. The spectra show the A_1(TO) modes.

splitting according to their large mode effective charges, while that of the TO2 and TO3 modes is much less affected by the electric field. Thus, the TO1, TO2, TO3 and TO4 modes can be, respectively, associated to the LO3, LO1, LO2 and LO4 modes.

Figure 2 compares the calculated Raman spectrum of $LiNbO_3$ and the experimental one obtained for a $x(zz)y$ scattering configuration. In such a configuration, the incoming photon has its wavevector along x and its polarization along z while the scattered photon has its wavevector along y and its polarization along z. Thus, only pure A_1(TO) modes can be detected in this configuration. We observe a qualitative good agreement between the calculated and experimental spectra. Indeed, the TO1 and TO4 modes are correctly predicted both in position and relative intensity, and have the strongest scattering efficiency. The TO2 mode appears weaker on the calculated spectrum than on the experimental one. However, this effect is not related to the intrinsic scattering efficiency of the TO2 mode. It is rather a consequence of the fact that the TO1 line in the experimental spectrum is quite broad and that it overlaps with the TO2 line, whereas this is not the case for the calculated spectrum since we use a constant linewidth to represent the Raman lines. Finally, the scattering efficiency of the calculated TO3 mode is weaker than that of the other modes in agreement with the experiment, although the calculated efficiency is so small that this line does not appear distinctly in panel B of figure 2. Thus, the four Raman A_1(TO) modes are unambiguously assigned by our calculations and are in agreement with the assignments reported in the literature.

4.2.2. E-modes. Frequencies of the calculated E(TO) and E(LO) modes are reported in table 4. The overlap matrix between the eigenvectors of the E(TO) and E(LO) modes, also reported in table 4, shows that the mixing between the LO and TO modes is important for all E(TO) modes except for the TO6 and TO9 modes for which this mixing is weak. These two latter E(TO) modes can therefore be associated to the LO5 and LO8 modes, respectively.

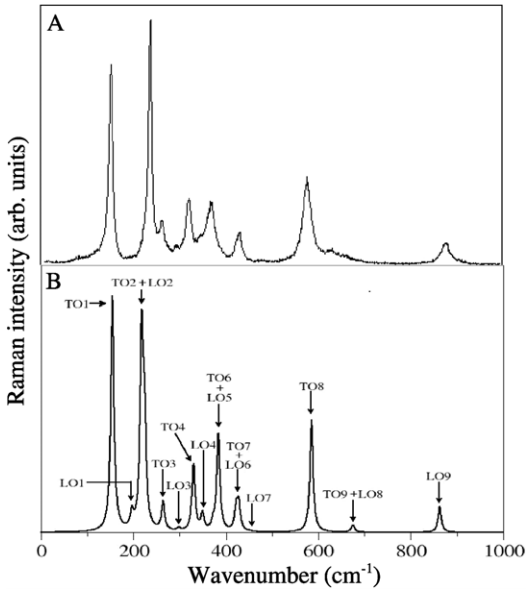

Figure 3. Experimental [6] (A) and calculated (B) Raman spectra of $LiNbO_3$ for a $x(yz)y$ scattering configuration in the 0–1000 cm^{-1} range. The spectra show the E(TO) and E(LO) modes.

Table 4. Overlap matrix between the eigenvectors of the E(LO) and E(TO) modes of $LiNbO_3$. Values in parentheses are the frequencies (in cm^{-1}) of the different E-modes, whereas the values in square brackets are the mode effective charges of the E(TO) modes.

		TO1 [4.620] (155)	TO2 [1.467] (218)	TO3 [3.610] (264)	TO4 [2.652] (330)	TO5 [2.341] (372)	TO6 [0.474] (384)	TO7 [0.942] (428)	TO8 [6.507] (585)	TO9 [1.105] (677)
LO1	(197)	**0.795**	0.480	0.338	0.098	0.097	0.002	0.014	0.063	0.008
LO2	(224)	0.316	**0.849**	0.407	0.082	0.077	0.002	0.011	0.046	0.005
LO3	(298)	0.302	0.159	**0.736**	0.484	0.301	0.006	0.035	0.125	0.014
LO4	(349)	0.135	0.059	0.192	**0.779**	0.568	0.010	0.039	0.103	0.011
LO5	(384)	0.002	0.001	0.002	0.004	0.024	**1.000**	0.001	0.002	0.000
LO6	(423)	0.092	0.036	0.102	0.129	0.328	0.010	**0.911**	0.160	0.015
LO7	(452)	0.229	0.088	0.243	0.279	0.597	0.017	0.402	0.532	0.046
LO8	(675)	0.031	0.011	0.028	0.024	0.038	0.001	0.009	0.175	**0.983**
LO9	(863)	0.311	0.108	0.268	0.219	0.325	0.008	0.072	**0.793**	0.179

Figure 3 compares the calculated and the experimental Raman spectrum of $LiNbO_3$ obtained for a $x(yz)y$ scattering configuration. In this configuration, only the E(TO) and E(LO) modes can be detected. As in case of the A_1-modes, a qualitative good agreement between the calculation and the experiment is observed both in the frequency position and the relative intensity of the Raman lines. However, in spite of this good agreement, the assignment of the nine Raman E(TO) modes remains difficult because many different experimental frequencies, with different assignments, have been reported in the literature (see table 5). This comes from the fact that the properties of $LiNbO_3$ crystals strongly depend on the internal and external defects [34], these small modifications in the structure and to the stoichiometry of the material being particularly sensitive in Raman spectroscopy. Nevertheless, most authors seem to agree on seven E(TO) modes centered around 152, 237, 265, 322, 368, 431 and 580 cm^{-1}. For the

Table 5. Frequencies (cm^{-1}) of the E(TO) modes in the $R3c$ phase of $LiNbO_3$.

	Calculated			Experimental								
				Raman						Infrared		
	Present	[8]	[9]	[6]	[30]	[7]	[31]	[29]	[32]	[29]	[35]	[36]
						92						
TO1	155	151	157	153	155	152	155	152	152[a]	152	155	147
		167		177	180							
TO2	218	236	214	238	238	238	238	238	236	236	238	234
TO3	264		269	264	265	262	265	264	263	265	265	258
TO4	330	307	349	322	325	322	325	321	322	322	324	317
TO5	372	334	419							363	361	354
TO6	384	352	423	369	371	368	371	367	370			
TO7	428	432	446	432	431	436	431	434	431	431	431	421
									530			537
TO8	585	526	605	580	582	582	582	579	578	586	582	
		617		610	610	630						
TO9	677		690				668			670[b]	668	657
							743					
											840	

[a] These authors suggest that there are two different modes at 152 cm^{-1}.
[b] Combination bands.

two missing Raman modes, different frequencies have been suggested both experimentally and theoretically. Experimentally, Ridah *et al* [6] and Repelin *et al* [30] suggest frequencies at 180 and 610 cm^{-1} which have been assigned by Barker *et al* [29] as mixed phonons that have their wavevector at 45° from the z-axis, Kaminow *et al* [7] report modes at 92 and 630 cm^{-1}, Claus *et al* [31] mention phonons at 668, also observed by infrared spectroscopy [29, 35, 36], and 743 cm^{-1} and Yang *et al* [32] report modes at 152 and 530 cm^{-1} and suggest that the frequencies at 743 and around 670 cm^{-1} are due to combination bands. Using first-principles calculations, Parlinski *et al* [9] found the seven modes reported by most authors as well as phonons at 423 and 690 cm^{-1}, while Caciuc *et al* [8] suggest the existence of phonons at 167 and 617 cm^{-1} as proposed by Ridah *et al* [6] and Repelin *et al* [30] (see table 5).

Inspection of table 5 shows that our calculation reproduces the seven modes mentioned above. For the two remaining modes, we suggest that (i) one of them has a frequency of about 670 cm^{-1} in agreement with [9, 29, 31, 35, 36] and (ii) the TO5 and TO6 modes are not the same experimental Raman mode but are two different E(TO) modes, the first mode only being visible by infrared spectroscopy and the second only being visible by Raman spectroscopy.

Panel B of figure 1 displays the calculated infrared reflectivity spectrum (without damping) at normal incidence of the E-modes. A good agreement between theory and experiment [29] is observed both for frequency and minima positions. In particular, the TO9 mode centered at 677 cm^{-1}, assigned experimentally by Barker *et al* [29] and Yang *et al* [32] to a combination band, is clearly observed in both our calculated infrared and Raman spectra, giving support to the idea that this mode does not result from a second-order process but from a first-order process. In addition, the TO9 mode is strongly damped because its reflection peak, calculated without damping, is more intense than the experimental [29] one, suggesting that this phonon mode can sometimes not be detected by Raman spectroscopy and has a broad and weak Raman line in the case where it is detected (see figure 3). Thus, the experimental Raman line around 670 cm^{-1}, which we assign to the calculated TO9 line, is the first missing E(TO) mode.

Table 6. Infrared (IR) mode oscillator strengths ($\times 10^{-4}$ au) (see footnote 2) and reduced Raman (Ra) scattering efficiencies of the E(TO) modes in $LiNbO_3$. Calculated and experimental reduced Raman efficiencies have been determined from the $x(zy)z$ configuration in which only the E(TO) modes are detected.

	Theory		Experiment	
Mode	IR S_m	Ra I/I_{TO1}	IR [29] S_m	Ra [6] I/I_{TO1}
TO1	5.89	1.00	6.02	1.00
TO2	0.55	0.82	0.53	0.97
TO3	4.38	0.12	4.58	0.21
TO4	2.72	0.28	2.70	0.30
TO5	3.60	0.03	3.59	
TO6	0.15	0.19		0.19
TO7	0.31	0.11	0.40	0.10
TO8	14.33	0.48	13.43	0.37
TO9	0.37	0.01	1.06	0.12

Calculated and experimental infrared mode oscillator strengths[2] of the E(TO) modes are reported in table 6 with their Raman scattering efficiencies and are relevant to clarify the longstanding debate in the experimental assignment of the last missing E(TO) mode. Because it is very difficult to determine accurately the absolute Raman scattering efficiencies experimentally, we have therefore reported the intensities of the Raman lines relative to the TO1 line intensity. The TO5 mode has an oscillator strength of 3.60×10^{-4} au, in very good agreement with the experiment, and a weak Raman scattering efficiency. Due to its significant mode oscillator strength, this mode is easily detected by infrared spectroscopy and it gives rise to a measurable LO–TO splitting (see figure 1). In contrast, this mode is difficult to detect by Raman spectroscopy. The TO6 mode has a weak oscillator strength and a significant Raman scattering efficiency, giving rise to the well-defined Raman line centered at 384 cm^{-1} in figure 3. In contrast, due to its weak mode oscillator strength, this mode is difficult to detect by infrared spectroscopy and it does not give rise to a notable LO–TO splitting (see figure 1). Thus, the distinct characteristics of the TO5 and TO6 modes give a first argument in favor of our assumption that there are two E(TO) modes around 370 cm^{-1}.

An additional argument in favor of our assumption comes from an experiment of Claus and co-workers [31]. These authors used Raman spectroscopy to measure the dependence of the phonon frequencies on the angle between the phonon wavevector, **q**, and the z-axis of $LiNbO_3$. They observed only one mode around 370 cm^{-1} with no angular dependence of the frequency, indicating that this mode has a negligible infrared oscillator strength. The characteristics of the mode measured by Claus *et al* are therefore compatible with the characteristics of the TO6 mode. These observations cannot be explained if we assume only one mode at this frequency because the oscillator strength of the TO5 mode (3.60×10^{-4} au) is not compatible with the absence of angular dispersion of the phonon frequency.

4.3. Influence of the $\tilde{d}$-tensor elements on the profile of the Raman spectra of LO modes

As discussed in section 2.2, knowledge of the $\tilde{d}$-tensor elements is *a priori* required to compute the intensity of the LO Raman lines in polar crystals (see equation (7)). However, calculations or measurements of the $\tilde{d}$-tensor elements are not always easy or possible. It is therefore useful

[2] The mode oscillator strength S_m of the mode m is given by [17]: $S_m = \sum_\alpha |\sum_{\kappa,\beta} Z^*_{\alpha\beta}(\kappa) u_m(\kappa\beta)|^2$.

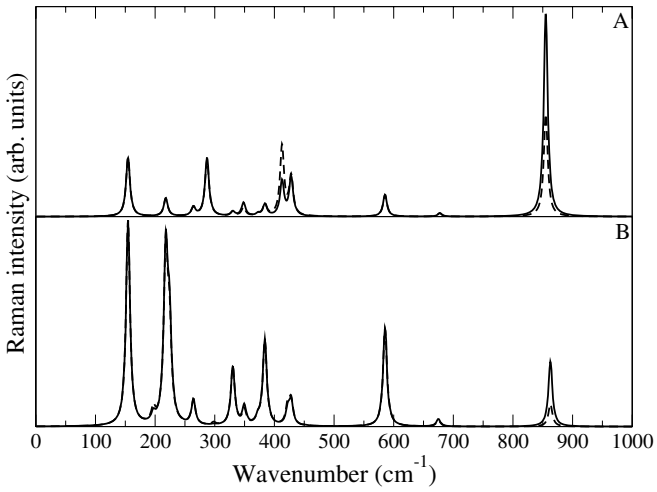

Figure 4. Influence on the Raman intensity of the LO lines of $LiNbO_3$ taking into account (dashed lines) or not (continuous lines) the $\tilde{d}$-tensor elements for a $z(yy)\bar{z}$ (A) and $x(zx)y$ (B) scattering configurations. In the first configuration the A_1(LO) and E(TO) modes are detected whereas the E(LO) and E(TO) are detected in the second one.

to investigate how the second term in the right-hand side of equation (7) affects the intensity of LO lines in the Raman spectrum of $LiNbO_3$. From equations (4) and (7), the profile of the Raman spectrum of $LiNbO_3$, in a configuration where the LO modes can be detected, should be significantly affected if the $\tilde{d}$-tensor elements and/or the mode effective charges are high (ϵ^{∞}_{xx} and ϵ^{∞}_{zz} being very close [20]).

The Raman intensity of the LO lines of the $R3c$ phase of $LiNbO_3$ can only be affected by the d_{22} and d_{31} independent elements of the $\tilde{d}$-tensor. Indeed, although the d_{33} term has the highest value (-30.21 pm V^{-1}), this term, involved from equations (9) and (10) in the detection of the A_1 modes, cannot affect the Raman intensity of the A_1(LO) modes due to the transverse polarization of the light. Thus, there is no configuration restricting pure A_1(LO) modes in $LiNbO_3$ monocrystals with Raman spectroscopy.

Figure 4 compares the calculated Raman spectrum of $LiNbO_3$ for a $z(yy)\bar{z}$ (panel A) and $x(zx)y$ (panel B) scattering configurations taking (or not taking) into account the correction to the second term in the right-hand side of equation (7). In the first configuration, the A_1(LO) and E(TO) modes are detected and the Raman intensity of the A_1(LO) modes are affected by the d_{22} and d_{31} terms. In the second configuration, the E(LO) and E(TO) modes are detected and the Raman intensity of the E(LO) modes are affected only by the d_{31} term. We observe that the Raman intensity of the LO lines is not altered except for the A_1(LO3), A_1(LO4) and E(LO9) lines, centered respectively at 413, 855 and 863 cm^{-1}, which are less intense taking into account the second term correction in the right-hand side of equation (7). This is because these LO modes have an overlap of 0.811, 0.897 and 0.793, respectively, with the A_1(TO1), A_1(TO4) and E(TO8) modes, which also have the higher mode effective charge (see tables 3 and 4). No significant modification in the Raman intensity of the LO modes of $LiNbO_3$ has been pointed out in other scattering configurations. Thus, knowledge of the $\tilde{d}$-tensor has only a minor effect on the profile of the Raman spectra of $LiNbO_3$ in a configuration where the LO modes are detected.

5. Conclusions

In this paper we have calculated, for the first time, the derivative of the linear optical susceptibility with respect to atomic displacement and the second-order nonlinear optical susceptibility tensors of the ferroelectric phase of $LiNbO_3$. These two quantities are found to be in good agreement with the experimental data, leading to an accurate calculation of the nonresonant Raman spectra of $LiNbO_3$ for different experimental configurations. Infrared reflectivity spectra of the ferroelectric phase of $LiNbO_3$ have been also calculated.

Then, we showed that the calculation of the infrared and Raman intensities of the ferroelectric phase of $LiNbO_3$ from first-principles is particularly relevant for clarifying the different controversies in the assignment of the E(TO) modes. Indeed, our calculation reproduces seven of nine experimental E(TO) modes centered around 152, 237, 265, 322, 368, 431 and 580 cm^{-1} in agreement with most authors. For the two remaining modes, we have shown that (i) one of them has a frequency of about 670 cm^{-1} wrongly assigned to a combination band in literature and (ii) the comparison of the calculated Raman scattering efficiencies and infrared mode oscillator strengths with the corresponding experimental values leads to the identification of two E(TO) modes around 370 cm^{-1}. This latter prediction has never been demonstrated in the previous studies, which assign only one E(TO) mode around this frequency. In addition, we have shown that the nonlinear optical susceptibility coefficients have a minor effect on the profile of the Raman spectra of $LiNbO_3$ in a configuration where the E(LO) modes are detected.

Finally, DFT, taking advantage of a recent implementation based on the nonlinear response formalism and the $2n+1$ theorem, appears as an efficient tool to calculate the Raman spectra of ferroelectric materials, and thus make reasonable predictions on the assignment of their phonon lines.

Acknowledgments

Calculations have been performed on the NIC (Université de Liège, Belgium) and at CISM (Université Catholique de Louvain, Belgium) with the financial support of FNRS (project FRFC No 2.4502.05 'Simulation numérique. Application en physique de l'état solide, océanographie et dynamique des fluides'). This work was supported by the VolkswagenStiftung, the European Network of Excellence FAME-NoE and the European strep MaCoMuFi.

References

[1] Nishihara H, Haruna M and Suhara T 1985 *Optical Integrated Circuits* (New York: McGraw-Hill)
[2] Buse K, Adibi A and Psalti D 1998 *Nature* **393** 665
[3] Hesselink L, Orlov S S, Liu A, Akella A, Lande D and Neurgaonkar R R 1998 *Science* **282** 1089
[4] Noiret I, Lefebvre J, Schamps J, Delattre F, Branier A and Ferriol M 2000 *J. Phys.: Condens. Matter* **12** 2305
[5] Boysen H and Altorfer F 1994 *Acta Crystallogr.* B **50** 405
[6] Ridah A, Bourson P, Fontana M D and Malovichko G 1997 *J. Phys.: Condens. Matter* **9** 9687
[7] Kaminow I P and Johnston W D Jr 1967 *Phys. Rev.* **160** 519
[8] Caciuc V, Postnikov A V and Borstel G 2000 *Phys. Rev.* B **61** 8806
[9] Parlinski K, Li Z Q and Kawazoe Y 2000 *Phys. Rev.* B **61** 272
[10] Veithen M, Gonze X and Ghosez Ph 2005 *Phys. Rev.* B **71** 125107
[11] Veithen M, Gonze X and Ghosez Ph 2004 *Phys. Rev. Lett.* **93** 187401
[12] Hughes J L P and Sipe J E 1996 *Phys. Rev.* B **53** 10751
[13] Kleinman D A 1962 *Phys. Rev.* **126** 1977
[14] Dal Corso A, Mauri F and Rubio A 1996 *Phys. Rev.* B **53** 15638
[15] Dal Corso A and Mauri F 1994 *Phys. Rev.* B **50** 5756

[16] Cardona M and Güntherodt G 1982 *Light Scattering in Solids II* (Berlin: Springer)
[17] Gonze X and Lee C 1997 *Phys. Rev.* B **55** 10355
[18] Hermet P, Izard N, Rahmani A and Ghosez Ph 2006 *J. Phys. Chem.* B **110** 24869
[19] Johnston W D Jr 1970 *Phys. Rev.* B **1** 3494
[20] Veithen M and Ghosez Ph 2002 *Phys. Rev.* B **65** 214302
[21] Gonze X, Beuken J M, Caracas R, Detraux F, Fuchs M, Rignanese G M, Sindic L, Verstraete M, Zerah G, Jollet F, Torrent M, Roy A, Mikami M, Ghosez Ph, Raty J Y and Allan D C 2002 *Comput. Mater. Sci.* **25** 478
[22] Perdew J P and Wang Y 1992 *Phys. Rev.* B **45** 13244
[23] Troullier N and Martins J L 1991 *Phys. Rev.* B **43** 1993
[24] Fuchs M and Scheffler M 1999 *Comput. Phys. Commun.* **119** 67
[25] Monkhorst H J and Pack J D 1976 *Phys. Rev.* B **13** 5188
[26] Dmitriev V G, Gurzadyan G G and Nikogosyan D N 1999 *Handbook of Nonlinear Optical Crystals* (Berlin: Springer)
[27] Wemple S H and DiDomenico D Jr 1972 *Appl. Solid State Sci.* vol 3 (New York: Academic)
[28] Kuzmany H 1998 *Solid-State Spectroscopy* (Berlin: Springer)
[29] Barker A S Jr and Loudon R 1967 *Phys. Rev.* **158** 433
[30] Repelin Y, Husson E, Bennani F and Proust C 1999 *J. Phys. Chem. Solids* **60** 819
[31] Claus R, Borstel G, Wiesendanger E and Steffan L 1972 *Z. Naturf.* a **27** 1187
[32] Yang X, Lan G, Li B and Wang H 1987 *Phys. Status Solidi* b **141** 287
[33] Ridah A, Fontana M D and Bourson P 1997 *Phys. Rev.* B **56** 5967
[34] Räuber A 1978 *Current Topics in Materials Science* vol 1 (Amsterdam: North-Holland)
[35] Schuller E, Claus R, Falge H J and Borstel G 1977 *Z. Naturf.* a **32** 47
[36] Axe J D and Kane D F O 1966 *Appl. Phys. Lett.* **9** 58